communications biology

A Nature Portfolio journal

Article

https://doi.org/10.1038/s42003-025-08398-w

A novel model of light-induced middle cerebral artery occlusion and recanalization in mice

Check for updates

Emilia Conti [1,2] ✉, Antea Minetti [3], Lapo Turrini [1,2], Noemi Carlini[3], Cristina Sarti[4], Anna Maria Gori[5], Elena Sticchi[5], Betti Giusti[5], Cristina Spalletti[3], Marzia Baldereschi[3], Anna Letizia Allegra Mascaro [2,3,7] & Francesco Saverio Pavone [1,2,6,7]

Ischemic stroke caused by the abrupt interruption of blood flow is one of the leading causes of death and disability worldwide. Despite expanding reperfusion treatment indications, a significant proportion of patients (54.5%) experiences poor outcomes, regardless of successful recanalization, emphasizing the need for clinically relevant preclinical stroke models to better understand the mechanisms associated with effective reperfusion. Here, we develop and characterize a novel mouse model of light-induced recanalization following the photothrombotic occlusion of the distal branch of the middle cerebral artery (MCA). The recanalization provides a meaningful reduction of the infarct volume compared to non-recanalized mice. Moreover, the generalized motor impairment is less severe, as measured by the Neuro Deficit score. Ex vivo investigation highlights that light-mediated recanalization mitigates astrocyte complexity in the periinfarct cortex of recanalized mice. Moreover, light-induced recanalization reduces cerebral edema occurrence. Finally, the investigation of circulating biomarkers shows that our model of occlusion and recanalization of the MCA recapitulates the neuroinflammatory cascade of the acute phase of ischemic stroke.

Therapeutic options to fight stroke are still limited, and tissue plasminogen activator and mechanical thrombectomy are up to now the only approved clinical treatments. The goal of these therapies is to induce the recanalization and the resulting reperfusion of the tissue through the restoration of the downstream capillary blood flow[1]. However, even in cases of complete vessel recanalization, not all patients achieved a favorable clinical outcome[2]. This phenomenon, termed "futile recanalization", often occurs when successful recanalization fails to bring favorable prognosis despite a perfect revascularization, and unitl now the underlying mechanisms of futile recanalizztion were not clear[3]. In this framework, the development of animal models recapitulating the essential features of stroke progression after recanalization[4] plays a key role, to further elucidate the insurgence of pathophysiological mechanisms after brain ischemia. Among the several models developed, the intraluminal suture of the middle cerebral artery (MCA), though characterized by high variability of the infarct size resulting in low reproducibility and an unsatisfactory success rate of occlusion[5], has become a widespread model for mimicking MCA occlusion in rodents. This model is able to reproduce neuronal cell death, cerebral inflammation, and blood-brain barrier (BBB) disruption and allows the recanalization of the blood vessel by removing the suture filament[5,6]. However, the sudden restoration of blood flow after the occlusion has been proven to be counterproductive to improve post-stroke recovery[7]. Other strategies have been proposed to overcome these limitations, in particular, Watson in 2002[8] characterized in rats a protocol to induce an ischemic stroke in the distal branch of the MCA through photothrombosis and recanalization by UV laser-mediated clot disruption. As previously described by Watson, the UV-mediated recanalization process is twofold: on one hand, this approach promotes vasodilation mechanisms, attributed to photoacoustic alterations of smooth muscle contractile proteins, promote blood perfusion; on the other hand, UV irradiation induces a reduction in thrombus density, promoting the formation of multiple microscopic, progressively enlarging channels in the thrombus that lead to the recanalization of platelet-occluded arteries[9,10]. However, light-mediated recanalization was never attempted in mice, which represent the main model for genetic manipulation. Recently,

[1]National Institute of Optics, National Research Council, Sesto Fiorentino, Italy. [2]European Laboratory for Non-Linear Spectroscopy (LENS), Sesto Fiorentino, Italy. [3]Neuroscience Institute, National Research Council, Pisa, Italy. [4]Neurofarba Department, University of Florence, Firenze, Italy. [5]Department of Experimental and Clinical Medicine, University of Florence, Firenze, Italy. [6]Department of Physics and Astronomy, University of Florence, Sesto Fiorentino, Italy. [7]These authors contributed equally: Anna Letizia Allegra Mascaro, Francesco Saverio Pavone. ✉e-mail: conti@lens.unifi.it

we elaborated in mice a novel model of photothrombotic occlusion of the distal branch of the middle cerebral artery[11] that allows the formation of a stable clot in the blood vessel, leading to reproducible extended damage in the mouse cortex one week after the lesion. The great advantage of the photothrombotic model is the capability to induce the recanalization of the targeted blood vessel by illuminating the occluded artery with a specific wavelength, as previously demonstrated in rats[8,9].

Here, we developed and characterized a novel model of light-induced recanalization after the photothrombotic occlusion of the distal branch of the MCA. This model is highly translational since: (i) the occlusion localization in one of the main sites of cerebral ischemia in humans (MCA), (ii) the formation of a platelet- and fibrin-rich thrombus in the irradiated site, and (iii) the possibility to revert the occlusion through light-mediated recanalization. In the first set of experiments, we characterized the light-induced occlusion and recanalization model by performing in vivo evaluations of mice behavior and body weight, and ex vivo evaluation of the lesion volume and astrocytes morphology through immunostaining, one week after stroke induction. To further enhance the translational value of this study, we investigated, in a second set of experiments, a panel of circulating biomarkers related to the inflammatory reaction 24 h after the ischemia and the occurrence of cerebral edema.

Results

All-optical occlusion and recanalization induce the reduction of lesion volume in mice

We developed a novel system to sequentially perform the permanent occlusion of the distal branch of the MCA and the recanalization of the blood vessel after 30 min of stable occlusion (Fig. 1a). We characterized the mouse model in the acute phase after injury by comparing recanalized mice (PTRC group, photothrombosis PT followed by recanalization RC) with non-recanalized stroke mice (PT group, photothrombosis, previously published in ref. 11) and with a Sham group (saline i.p. injection followed by green laser illumination and UV LED illumination), as shown in Fig. 1b. In a recent work[11], we characterized the photothrombotic occlusion model of the distal MCA, obtained by illuminating the target blood vessel with a green laser for 25 min after the injection of the photosensitive dye Rose Bengal, to induce a stable occlusion (Fig. 1c first three panels). The custom-made apparatus (Fig. 1a) is equipped with two illumination sources, a green laser and a UV LED, for blood vessel occlusion and recanalization, respectively. The system allows displacing the animal between the two illumination foci through a slit. 30 min after the green light-mediated occlusion, illumination of the distal MCA with UV light for 15 min promoted the recanalization of the blood vessel (Fig. 1c right panel). The occlusion of the distal branch of the MCA followed by UV recanalization is lethal for 6.6% ($n = 1$) of mice one day after irradiation and 13.3% ($n = 2$) one week after stroke (Supplementary Fig. 1b).

Lesion volume quantification was performed 7 days after the stroke. The NeuN immunostaining on PTRC brain coronal sections (Fig. 1d) highlighted a region of dead tissue affecting only the mouse cortex, extending from motor regions up to visual areas, in the rostrocaudal direction, with an overall lesion volume of 4.820 ± 0.2 mm^3 (Fig. 1e). Spared neuronal cells could be detected in the ischemic core following recanalization (Supplementary Fig.1c). Sham mice showed no sign of tissue suffering due to craniotomy and laser or LED irradiation. Recanalization resulted in a 31% reduction of the infarct size, with respect to non-recanalized mice (PT = 100.00 ± 2.01 and PTRC = 69.01 ± 2.84, Fig. 1f). Finally, we evaluated the impact of the ischemic insult across the functional areas of the mouse cortex revealing that the damage predominantly affected the somatosensory area (Fig. 1g and Supplementary Fig. 1d).

MCA recanalization promotes the recovery of the motor impairment 1 week after the injury

Based on our previous study, where the MCA permanent occlusion induced a severe motor dysfunction, we administered a battery of motor tests (see Method section) to assign a neuro deficit score in PTRC mice (NDS, Fig. 2a left panel). The animals of all experimental groups received an NDS of 0 during baseline assessment. 24 h after the lesion, both the PT and PTRC groups showed a significant NDS increase compared with Sham mice at the same time point and with pre-stroke condition. More in detail, recanalization in PTRC mice resulted in a relevant reduction of motor impairment 24 h after the injury, significantly different from the PT group. The behavioral deficit of both groups was partially recovered one week after the photothrombosis, however, PTRC behavioral performances were still significantly better compared to PT mice (Fig. 2a left panel). Body weight was not altered in PT or PTRC mice (Fig. 2a right panel).

Finally, to assess possible cognitive deficits in PTRC mice, we used the novel object recognition (NOR) test (Fig. 2b). During the habituation phase, the animal velocity and the time spent in movement were comparable between the two groups (Fig. 2c) suggesting that motor capabilities of Sham and PTRC mice were equivalent. Conversely, as highlighted by the exemplary trajectories shown in Fig. 2d, PTRC mice were characterized by a significantly lower novel object exploration time ratio (Fig. 2e left panel) and a lower discrimination index (Fig. 2e right panel) during the testing phase. Due to the severe motor impairment revealed in stroke mice without recanalization, it was not possible to perform the NOR test in the PT group.

These results are coherent with previous assessments of lesion location (Fig. 1g) indicating that only a small portion (3.83%) of the motor cortex is affected by the injury. Consequently, locomotion capability was preserved following MCA recanalization, as observed in the NOR habituation phase. In contrast, the extensive damage to the somatosensory cortex (70.76%), including the barrel field, likely explains the loss of discrimination capability observed in PTRC animals.

MCA recanalization partially mitigates post-stroke astrocytes complexity

Several studies suggest that neuroinflammation plays a role in the poor outcome of stroke patients with successful recanalization[12]. To evaluate the extent of cortical inflammation induced by MCA recanalization, we analyzed the distribution of astrocytes and their morphology through ex vivo immunofluorescence experiments (Figs. 3 and 4). In line with our recent work[11], we identified five regions of interest (ROI) within the cortex: ipsilesional ischemic border zone (IBZ_{IL}), remote zone (RZ_{IL}), contralesional ischemic border zone (IBZ_{CL}), and contralesional ischemic core (IC_{CL}) (Fig. 3a).

By quantifying the astrocyte density in the aforementioned ROIs, we found a significant increase of GFAP-positive astrocytes in the peri-infarct area (IBZ_{IL}) with respect to all the other regions analyzed (Fig. 3b). Conversely, Sham mice presented a similar density of GFAP-positive cells in all the ROIs investigated (Supplementary Fig. 2a). Indeed, the comparison with the PTRC group highlighted a significant increase in astrocyte density in all the regions observed compared to Sham mice (Supplementary Fig. 2b). Contrary to what was previously observed in mice without recanalization, we revealed the presence of astrocytes in the ischemic core. Indeed, the comparison between the occlusion model (PT mice) and the recanalized one (PTRC mice) highlighted a significant increment of GFAP-positive cells in the ischemic core and in the peri-infarct region of the cortex (Fig. 3c). Hence, recanalization promotes astrocyte survival and may contribute to their increased presence in the perilesional cortex.

Then to investigate astrocyte morphology we first performed the Sholl analysis (Fig. 4a). As shown in Fig. 4b, we observed a significant increment of the intersections' number (9–30 μm from the cell body) of IBZ_{IL} astrocytes compared to other regions of PTRC mice (Fig. 4b). The comparison between photothrombotic-occluded and recanalized animals showed that astrocytes of PTRC mice presented an overall lower (even if not significant) number of intersections except for a slight increase (even if not significant) in the more distal regions to the cell body compared to occluded mice (Fig. 4c). Conversely, in Sham animals, Sholl analysis did not reveal any differences between the ROIs at increasing distances from the cell body (Supplementary Fig. 4a).

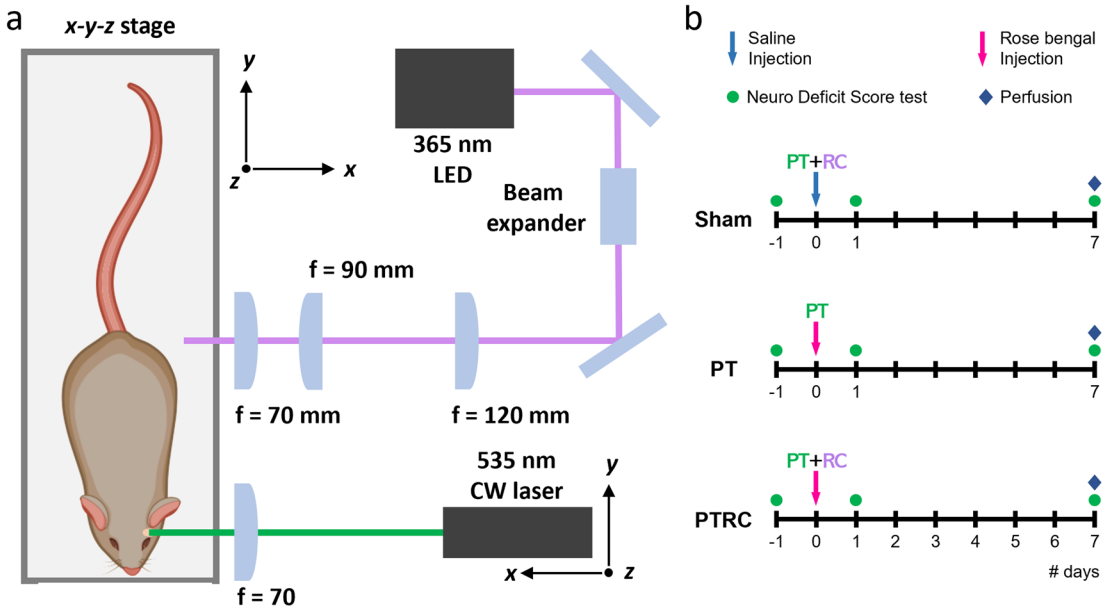

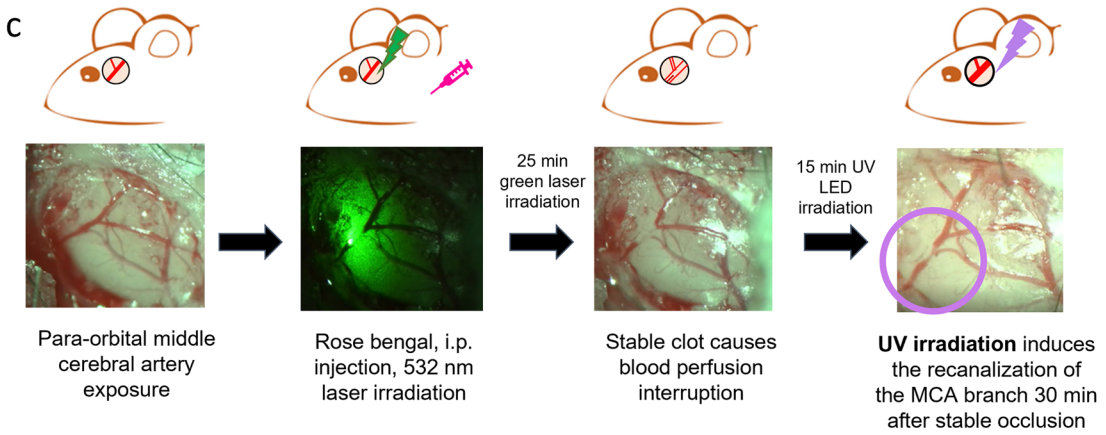

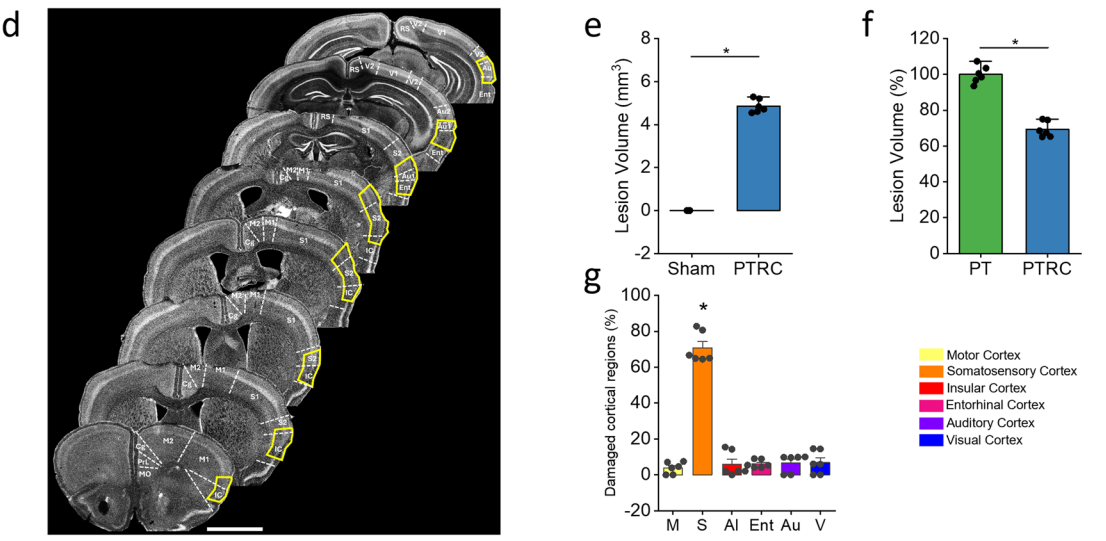

Finally, we performed the Skeleton analysis (Fig. 4d and Supplementary Fig. 3a) to quantify the length of astrocytic processes as well as the number of branches, junctions, and end-points. A modest increase in astrocyte complexity around the infarct (IBZ_{IL}) was due to an increment in total branch length (statistically significant compared to IC and IBZ_{CL}), number of branches (statistically significant compared to the IC), and number of junctions (statistically significant compared to the IC). The comparison between occluded and recanalized mice highlighted a significant increase in astrocyte complexity (number of branches, junctions, and end-points) without recanalization (PT group), although GFAP-positive cells of PTRC mice showed an increment of branch length compared to PT mice (Fig. 4e and Supplementary Fig. 3b). Skeleton analysis for

Fig. 1 | An all-optical system for occlusion-recanalization in mice. **a** Representative scheme of the custom-made setup for photothrombotic occlusion of the distal branch of the MCA and the recanalization of the occluded blood vessel, see methods for details. **b** Experimental timeline for Sham ($n = 3$), PT ($n = 6$), and PTRC ($n = 6$) mice. **c** Representative scheme of the main steps of photothrombotic occlusion and recanalization of the distal branch of the MCA (upper row) and corresponding images acquired during surgery (lower row). The first panel shows the exposure of the MCA after craniotomy; the second and the third panels are relative to the laser irradiation, followed by the formation of the clot; the last panel illustrates the recanalization of the MCA after UV LED irradiation. Scale bar 0.5 mm. **d** Representative subsequent coronal sections stained with NeuN showing the location and extension of lesioned areas (contoured by the yellow line). Scale bar, 2 mm. **e** Quantification (mean ± standard error of the mean, SEM) of stroke volume for the Sham (0.0 ± 0.0 mm^3) and PTRC groups (4.9 ± 0.3 mm^3) 1 week after photothrombosis; $F_{(1, 7)} = 675.212$, $^*p < 0.0001$ unpaired *t*-test (Sham $n = 3$ and PTRC $n = 6$). All data points for the Sham group are depicted as zero, indicating no observable lesion. Error bars, representing the SEM, are below the minimum threshold and thus not visible in the graph. **f** The bar plot highlights the comparison of stroke volume between PT and PTRC groups, normalized to the PT group (PT = 100.0 ± 2.0; PTRC = 69.3 ± 1.8); $F_{(1, 10)} = 128.949$, $^*p < 0.0001$ unpaired *t*-test (PT $n = 6$ and PTRC $n = 6$). **g** The bar plot shows the quantification in percentage of cortical regions affected by the damage. $^*p$ value based on One-way ANOVA ($F_{(5, 30)} = 123.161$) followed by post hoc Tukey HSD test: S-M $p < 0.0001$; S-IC $p < 0.0001$; S-Ent $p < 0.0001$; S-Au $p < 0.0001$; S-V $p < 0.0001$.

the Sham group did not show any significant differences in astrocyte morphology comparing ROIs from both the ipsilateral and contralateral hemispheres (Supplementary Fig. 4b–h).

In summary, we observed a significant increase in GFAP-positive astrocytes in the peri-infarct area and a significant decrease in the morphological complexity following recanalization compared to occlusion alone. Notably, the presence of GFAP-positive cells in the ischemic core was detected exclusively in stroke mice with recanalization. These findings indicate that recanalization modulates astrocyte distribution and reactivity, contributing to their increased presence in the perilesional cortex.

Recanalization attenuates microglial activation and phagocytosis in the perilesional cortex following ischemic stroke

Neuroinflammation plays a pivotal role in secondary injury progression following stroke, with both astrocytes and microglia contributing to the post-ischemic environment. To further characterize the inflammatory response in the perilesioned area, we analyzed microglial activation and phagocytic activity through double-labeling immunofluorescence for Iba1 (microglia) and CD68 (phagocytic marker) (Fig. 5).

Our results show that microglial density (Iba1+ cells/mm^2) was significantly increased in PT mice compared to Sham, while PTRC treatment significantly reduced microglial density compared to PT. Similarly, microglial activation (Iba1+ area) and phagocytic activity (CD68+ area) were markedly elevated in PT mice compared to Sham, with a significant reduction following recanalization. These findings suggest that recanalization modulates post-stroke neuroinflammation by attenuating microglial proliferation, activation, and phagocytosis, potentially contributing to a more controlled inflammatory response.

Together with the observed changes in astrocyte complexity, these results indicate that recanalization not only influences astrocyte morphology but also reduces microglial activation, reinforcing its potential role in modulating the neuroinflammatory milieu following ischemic stroke.

Timely recanalization of occluded MCA reduces the insurgence of cerebral edema

Animal studies suggest that reperfusion after endovascular treatment may increase the occurrence of cerebral edema, one of the most frequent stroke complications in humans[13]. In a separate set of experiments, we first assessed whether our model of MCA occlusion presented cerebral edema; then we asked if LED-mediated recanalization could reduce this secondary damage. To this aim, we evaluated the brain water content of ipsilesional and contralesional hemispheres (as in ref. 14) as a measure of cerebral edema in the acute phase after stroke (Fig. 6a).

Mice of the three experimental groups (Sham, PT, and PTRC, Fig. 6b) were sacrificed 24 hours after the surgery. The mouse brain was cut along the midline to evaluate the wet weight (WW) of the ipsilesional and contralesional hemispheres. Samples were then incubated at 60 °C for 72 h and then weighed to obtain dry weight (DW). The comparison of the left and right hemispheres in Sham mice (Fig. 6c) did not reveal any difference in the brain water content suggesting that the surgery itself did not induce a strong inflammation, BBB leakage, and cerebral edema eventually. Conversely, a statistically significant increment of the percentage of water in the ipsilesional hemisphere was visible 24 h after the injury in PT mice. Moreover, the comparison between the operated/ipsilesional hemispheres of Sham and PT mice respectively highlighted a significant increase in the brain water content. Finally, we observed a reduction in the brain water content of the injured hemisphere in PTRC compared to PT mice, while no differences were found between the ipsilesional and contralesional hemispheres of PTRC mice. The evaluation of body weight variation and NDS (Fig. 6d, e) showed results comparable with those observed in the Stroke group (Fig. 2b). To conclude we observed a strong correlation between cerebral edema occurrence and motor impairment (Fig. 6f). These findings confirmed that the light-induced model of MCA occlusion faithfully reproduced short-term stroke complications such as cerebral edema, as shown in our previous work[11]. Here we found that the recanalization mediated by UV light drastically reduced the cerebral edema occurrence.

Circulating biomarkers analysis reveals a strong proinflammatory response in stroke mice lacking recanalization

Shortly after the onset of a stroke, damaged brain tissue releases proinflammatory molecules, such as cytokines and chemokines, which can be quantified from the peripheral venous blood[15]. Since this approach is commonly applied in clinical settings to stroke patients, the evaluation of circulating biomarkers in mice has a high translational potential[3]. Compared to human patients, the mouse model provides the additional benefit of allowing comparison with pre-stroke levels, which is highly informative on the absolute variation of the biomarker concentrations. Therefore, we performed a longitudinal analysis to monitor circulating biomarkers in peripheral mouse blood of the same mice where we assessed edema formation. Blood samples were collected from the retroorbital sinus at three time points, two weeks before (Pre), right after (Basal), and 1 day after (24 h) the surgery (see Fig. 6b for time point reference). To dampen the high intrinsic variability of protein serum concentration[16], we quantified the variation (delta) of the concentrations between two time points (Basal-Pre, 24h-Pre, and 24h-Basal). By comparing Basal and Pre time points, we found a significant increment of CCL3 and IL-6 proteins in the PT group with respect to Sham mice (Fig. 7a, b). In addition, we observed a significant increment of IL-6 in a late time window comparing 24 h and Pre, in PT mice with respect to Sham mice (Fig. 7b). In summary, the comparison between Sham control and PT stroke highlighted a strong increment of proinflammatory cytokines in the early phase after the insult.

Furthermore, the comparison between PT and PTRC mice revealed a significant rise of the proinflammatory cytokine ICAM-1/CD54, 24 h after stroke in non-treated mice (Fig. 7c). Finally, we found a significant increase of the cytokine IL-10 in the PT group compared to PTRC (Fig. 7d) right after stroke induction. No significant differences were observed in IL-1, IL-12, VEGF, and TNF-α evaluation (Supplementary Fig. 5). The analysis of circulating biomarkers highlighted that while in PT mice the MCA occlusion triggered a strong inflammatory response, recanalization is able to reduce the inflammatory reaction. This result might explain the decrease in cerebral edema occurrence in PTRC mice.

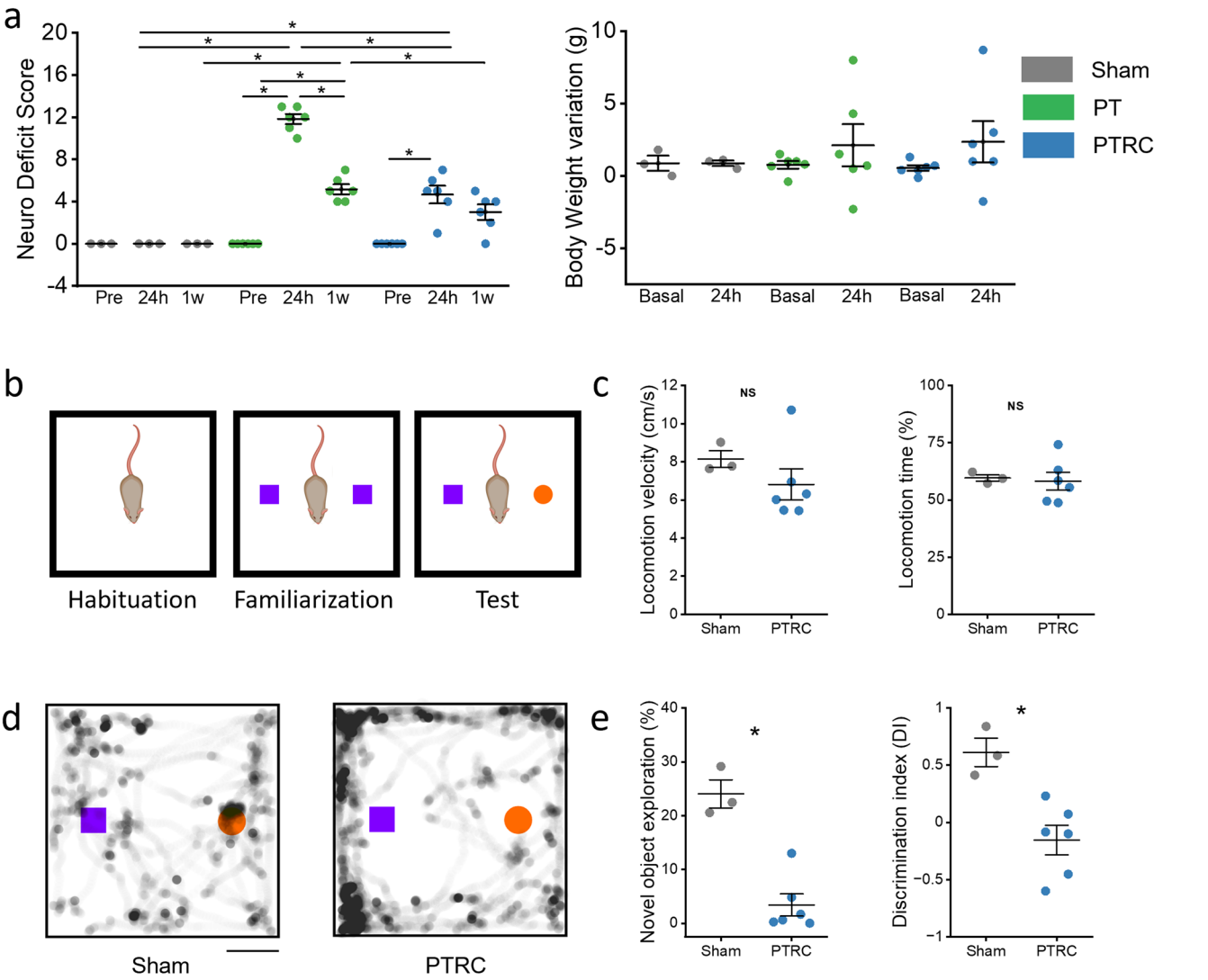

Fig. 2 | MCA recanalization promotes the recovery of the motor impairment 1 week after the injury. a The graph highlights an increase in neurological deficit scores in the Sham, PT, and PTRC groups 24 h and 1 week after surgery. Following mean and SEM values in the different experimental groups: Pre: Sham = 0, PT = 0, PTRC = 0; 24 h: Sham = 0; PT = 11.8 ± 0.5; PTRC = 4.7 ± 0.8; 1w: Sham = 0; PT = 5.2 ± 0.5; PTRC = 3.0 ± 0.7. *p value based on Two-way ANOVA repeated measure ($F_{(8, 6)} = 88.958$) followed by post hoc Tukey HSD test: PT Pre-24h $p < 0.00000001$; PT Pre-1w $p < 0.00001$; PT 24h-1w $p < 0.0000001$; PTRC Pre-24h $p = 0.004$; Sham 24h-PT 24 h $p < 0.0000001$; Sham 24h-PTRC 24 h $p = 0.004$; PT 24h-PTRC 24 h $p < 0.000001$; Sham 1w-PT 1w $p < 0.0001$; PT 1w-PTRC 1w $p = 0.02$. The graph in the right panel shows the variation of mice's body weight by comparing three time points Pre, 24 h and 1 week after the surgery (24 h indicates the variation between 24 h and Pre time points, 1w the variation between 1 week and 24 h time points). Following mean and SEM values in the different experimental groups: Sham: 24 h = 0.87 ± 0.5; 1w = 0.87 ± 0.2; PT: 24 h = 0.8 ± 0.3; 1w = 2.2 ± 1.5; PTRC: 24 h = 0.5 ± 0.2; 1w = 2.3 ± 1.4. **b** Representative scheme of Novel Object Recognition Test: habituation in an empty arena, familiarization with two identical objects (purple squares), testing with a new object (orange circle) replacing one of the familiar objects. **c** Quantification of mice locomotion velocity (Sham = 8.143 ± 0.441 cm/s; PTRC = 6.813 ± 0.813 cm/s) and locomotion time (Sham = 59.595 ± 1.413%; PTRC = 58.206 ± 3.881%). **d** Tracking of representative Sham and PTRC mice during 5 min of novel object exploration on the testing day. Individual coordinates of the center of mass of the animals are presented as a semi-transparent black dot. Increasing color intensity means that the animal spent more time in that area of the arena. Sham mouse spent more time investigating the novel object while PTRC mouse explored the border of the arena. **e** The left panel shows the percentage of time over the entire test spent exploring the novel object in Sham and PTRC groups (Sham = 24.050 ± 2.601; PTRC = 3.402 ± 2.051) p value based on One-way ANOVA ($F_{(1, 7)} = 35.788$) followed by post hoc Tukey HSD test *$p = 0.0005$; the right panel shows the discrimination index for Sham and PTRC mice (Sham = 0.612 ± 0.124; PTRC = −0.232 ± 0.103), p value based on One-way ANOVA ($F_{(1, 7)} = 24.452$) followed by post hoc Tukey HSD test *$p = 0.0017$.

Discussion

Stroke remains a significant global health burden, with limited therapeutic options beyond tissue plasminogen activator and mechanical thrombectomy, both aimed at recanalizing occluded vessels to restore blood flow and tissue perfusion[17]. However, growing evidence suggests that clot removal and vessel recanalization do not always result in tissue reperfusion, "no-reflow phenomenon"[18], leading to an unfavorable clinical outcome for the 30–68% of patients[19,20]. Moreover, the restoration of blood flow, particularly in large vessel occlusion, can lead to reperfusion injury, exacerbating tissue damage and impairing functional outcomes[21,22]. This fact underscores the importance of developing animal models of brain ischemia that faithfully recapitulate key features of stroke progression to better understand the underlying pathophysiological mechanisms. In this framework, the thromboembolic model developed by Orset and colleagues[4] represents a valuable translational approach to study the pathophysiology of the neurovascular milieu after stroke. However, injecting thrombin into the distal branch of the MCA may indeed lead to the formation of secondary microthrombi in smaller vessels or capillaries. While reperfusion treatment may mitigate some effects, the possibility of microinfarcts still exists. Alternative approaches, such as photothrombosis combined with laser-

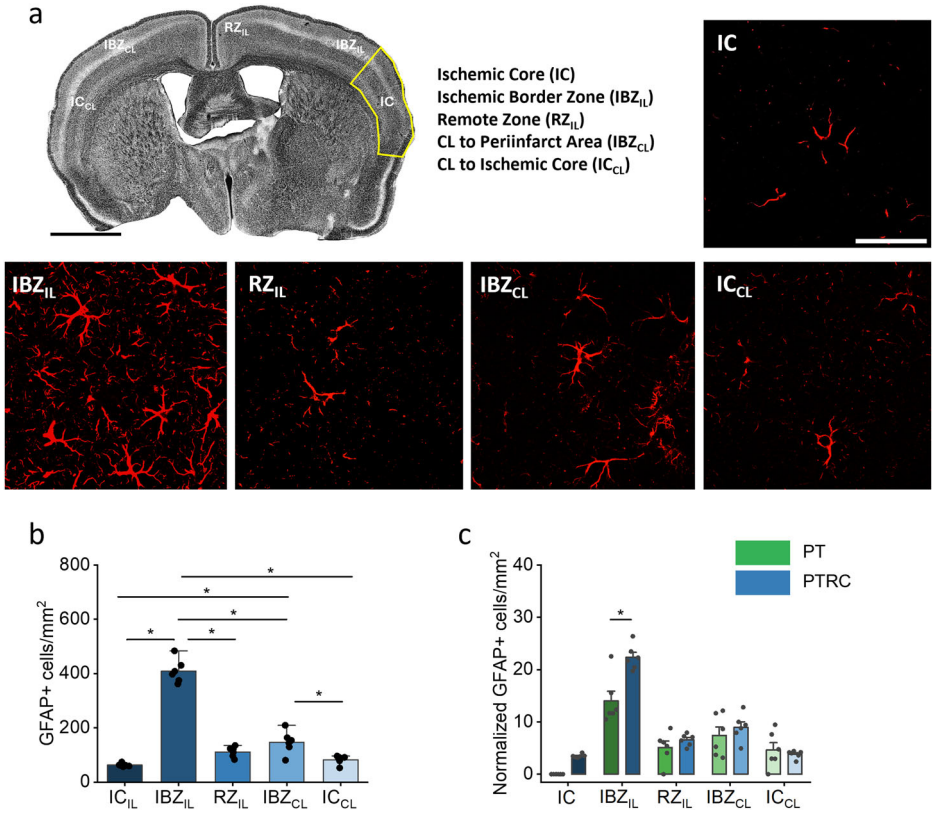

Fig. 3 | Astrocytes density in PTRC mice. a A representative brain slice highlighted the 5 ROIs identified for the astrocytes analysis. Scale bar 1 mm. Representative confocal field of views of each of the ROIs. Scale bar, 50 µm. **b** The graph shows the density (mean ± SEM) of GFAP-positive cells in the 5 ROIs for PTRC group $n = 6$ (IC = 63 ± 2; IBZ_{IL} = 409 ± 18; RZ_{IL} = 111 ± 8; IBZ_{CL} = 147 ± 17; IC_{CL} = 82 ± 6). *p value based on one-way ANOVA followed by Tukey's post hoc test for the intragroup statistical analysis (IC vs IBZ_{IL} $p < 0.0001$; IBZ_{IL} vs RZ_{IL} $p < 0.0001$; IBZ_{IL} vs IBZ_{CL} $p < 0.0001$; IBZ_{IL} vs IC_{CL} $p < 0.0001$; IBZ_{CL} vs IC_{IL} $p = 0.0003$; IC_{CL} vs IBZ_{IL} $p = 0.007$). **c** The graph shows the density (mean ± SEM) of GFAP-positive cells in the 5 ROIs normalized by the Sham group for both experimental groups (in green PT $n = 6$ and in blue PTRC $n = 6$). *p value based on two-way ANOVA followed by a post hoc Sidak's HSD test for the intergroup statistical analysis (PT vs PTRC IBZ_{IL} $p < 0.0001$). IC ischemic core, IBZ_{IL} ischemic border zone ipsi-lateral, RZ_{IL} remote zone ipsi-lateral, IBZ_{CL} ischemic border zone contra-lateral, IC_{CL} ischemic core contra-lateral.

induced clot disruption[23], offer opportunities for controlled occlusion and recanalization. Indeed, photothrombosis occurs only in the irradiation site, which in our experiments is inside the MCA. Moreover, the photothrombotic stroke model is based on functional endothelial damage caused by an intravascular photochemical reaction, which triggers a platelet-mediated response to cerebral vessel injury[9,24]. This results in a thrombus composed of platelets and fibrin, resembling those observed in clinical settings. In this study, we introduced a novel model of photothrombotic occlusion of the distal MCA in mice, allowing for the formation of a stable clot and subsequent recanalization through targeted LED-based illumination. A great advantage of our light-induced recanalization approach is the capability of being applied to different stroke animal models (such as the endothelin or thrombin model). Moreover, LED-mediated recanalization has great translational potential since integrating this approach with endoscopic treatment might possibly offer a versatile solution for achieving recanalization in stroke patients.

Our results demonstrate a striking reduction in infarct size and improved functional outcomes following recanalization compared to non-recanalized mice. Moreover, the novel object recognition test highlights the lack of discrimination capability between a familiar object and a novel one after the insult. Our study findings also provide valuable insights into the dynamics of cortical inflammation following middle cerebral artery photothrombotic occlusion and recanalization. Our results demonstrated a significant increase in GFAP-positive cell density in the peri-infarct area compared to other regions analyzed, indicating a localized astrocytic response to ischemic insult. Interestingly, contrary to previous observations in mice without recanalization[11], we detected the presence of astrocytes in the ischemic core. This unexpected finding suggests a potential role of astrocytes in the core region, possibly contributing to the modulation of the ischemic microenvironment[25,26].

Further investigations of astrocyte morphology using Sholl and Skeleton analysis[27,28] revealed significant differences in the morphology of astrocytic processes between regions and increased structural complexity in the perilesional region compared to ischemic core in stroke mice following recanalization[27,29]. Importantly, recanalized mice exhibited reduced astrocyte complexity compared to occluded mice, indicating a less complex morphological profile following recanalization[30]. The detection of GFAP-positive cells within the ischemic core and the observed increase in density and morphological complexity in the perilesional cortex suggest that MCA recanalization may enhance astrocyte survival. Such mechanisms may potentially play a role in enhancing post-stroke recovery. In parallel, our findings of attenuated microglial activation and phagocytosis in recanalized mice further support the notion that recanalization modulates the neuroinflammatory response following stroke. The coordinated reduction in astrocyte complexity and microglial activation highlights a broader anti-inflammatory effect of recanalization, which may contribute to limiting secondary injury and supporting neural repair. Consequently, our findings emphasize the potential therapeutic implications of modulating neuroinflammation through timely recanalization, which may represent a critical mechanism for promoting functional recovery, while also highlighting its potential relevance to other therapeutic strategies in clinical practice[31–36].

Moreover, recanalization was associated with cerebral edema reduction, further supporting the neuroprotective effects of controlled reperfusion[37]. Notably, we found a strong correlation between motor impairment and the occurrence of cerebral edema, suggesting that the severity of cerebral edema could be a predictor of post-stroke functional outcome[38].

Finally, to increase the translational bond with clinical research, we evaluated a panel of circulating biomarkers commonly assessed in post-stroke clinical practice. In this regard, the mouse model offers several advantages. One significant benefit is the ability to compare pre- and post-stroke conditions within the same subject, which helps normalize parameters and reduce inter-subject variability. More in detail, we performed a longitudinal investigation to assess the inflammatory response in the three experimental groups. Previous works investigated circulating biomarkers through terminal collection of blood through cardiac puncture[39,40] or ex vivo quantification[41]. This novel approach has the great advantage of providing the evaluation of biomarkers variation over time to understand the possible

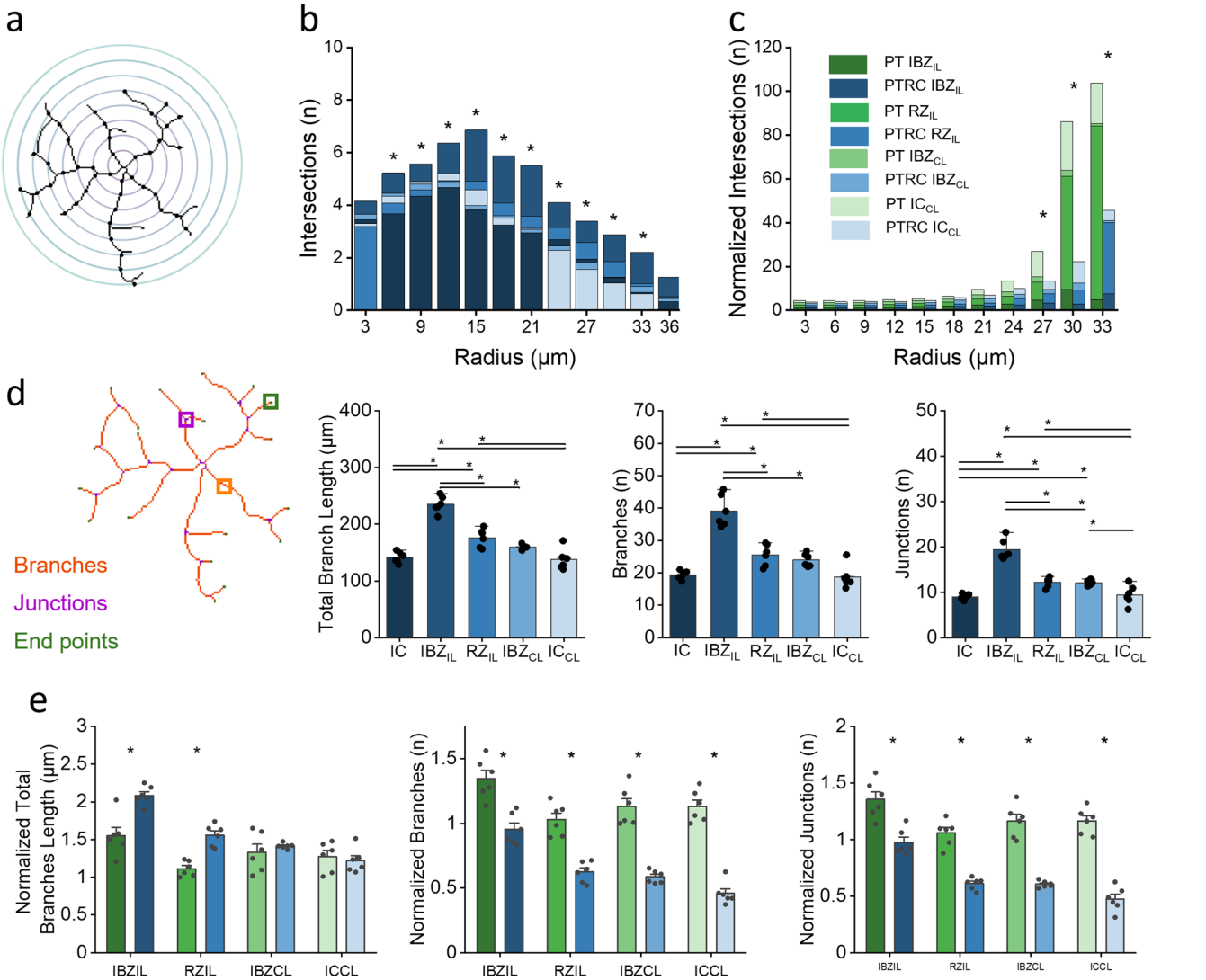

Fig. 4 | Comparison of morphological analysis between PT and PTRC. **a** Representative image of an astrocyte analyzed with the Sholl method for PTRC group ($n = 6$). **b** The graph shows the distribution of the number of intersections for each radius in the 5 ROIs for PTRC group (mean ± SEM). *p value based on two-way ANOVA followed by Tukey's post hoc test (6 μm: IC vs IBZ_{IL} $p < 0.0001$, IBZ_{IL} vs RZ_{IL} $p = 0.022$; 9 μm: IC vs IBZ_{IL} $p = 0.0059$; 12 μm: IC vs IBZ_{IL} $p < 0.0001$, IBZ_{IL} vs RZ_{IL} $p = 0.0001$, IBZ_{IL} vs IBZ_{CL} $p < 0.0001$, IBZ_{IL} vs IC_{CL} $p = 0.0163$; 15 μm: IC vs IBZ_{IL} $p < 0.0001$, IBZ_{IL} vs RZ_{IL} $p < 0.0001$, RZ_{IL} vs IC $p = 0.0478$, IBZ_{IL} vs IBZ_{CL} $p < 0.0001$, IBZ_{IL} vs IC_{CL} $p < 0.0001$; 18 μm: IC vs IBZ_{IL} $p < 0.0001$, IBZ_{IL} vs RZ_{IL} $p = 0.0013$, IBZ_{IL} vs IBZ_{CL} $p < 0.0001$, IBZ_{IL} vs IC_{CL} $p < 0.0001$; 21 μm: IC vs IBZ_{IL} $p < 0.0001$, IBZ_{IL} vs RZ_{IL} $p < 0.0001$, IBZ_{IL} vs IBZ_{CL} $p = 0.0001$, IBZ_{IL} vs IC_{CL} $p < 0,0001$; 24 μm: IC vs IBZ_{IL} $p = 0.0001$, IBZ_{IL} vs IBZ_{CL} $p < 0.0001$, IBZ_{IL} vs IC_{CL} $p < 0.0001$; 27 μm: IC vs IBZ_{IL} $p < 0.0001$, IBZ_{IL} vs IBZ_{CL} $p < 0.0001$, IBZ_{IL} vs IC_{CL} $p < 0.0001$; 30 μm: IC vs IBZ_{IL} $p < 0.0001$, IBZ_{IL} vs IBZ_{CL} $p < 0.0001$, IBZ_{IL} vs IC_{CL} $p < 0.0001$; 33 μm: IC vs IBZ_{IL} $p < 0.0001$, IBZ_{IL} vs RZ_{IL} $p = 0.0125$, IBZ_{IL} vs IBZ_{CL} $p = 0.0014$ IBZ_{IL} vs IC_{CL} $p < 0.0001$). **c** The graph shows the distribution of the number of intersections for each radius normalized by the Sham control group in the 4 ROIs for both experimental groups (in green PT $n = 6$ and in blue PTRC $n = 6$). *p value based on two-way ANOVA followed by Tukey's post hoc test (27 μm: PT vs PTRC RZ_{IL} $p = 0.0005$; 30 μm: PT vs PTRC IBZ_{IL} $p < 0,0001$; PT vs PTRC RZ_{IL} $p < 0.0001$; PT vs PTRC IC_{CL} $p < 0.0001$; 33 μm: PT vs PTRC IBZ_{IL} $p < 0.0001$; PT vs PTRC RZ_{IL} $p < 0.0001$; PT vs PTRC IBZ_{CL} $p < 0.0001$). **d** Representative image of the same astrocyte presented in (**a**), analyzed with the Skeleton analysis. The graphs (mean ± SEM) represent the morphological features of astrocytes in the 5 ROIs(- Total Branch Length: IC = 141.3 ± 3,9, IBZ_{IL} = 235.2 ± 5.9, RZ_{IL} = 176.0 ± 6.5, IBZ_{CL} = 159.7 ± 1.6, IC_{CL} = 137.6 ± 7.5; Branches: IC = 19.2 ± 0.5, IBZ_{IL} = 39.0 ± 2.0, RZ_{IL} = 25.5 ± 1.3, IBZ_{CL} = 24.0 ± 0.8, IC_{CL} = 18.7 ± 1.4; Junctions: IC = 9.0 ± 0.2, IBZ_{IL} = 19.4 ± 0.9, RZ_{IL} = 12.2 ± 0.4, IBZ_{CL} = 12.0 ± 0.2, IC_{CL} = 9.4 ± 0.9; End-points: IC = 10.2 ± 0.2, IBZ_{IL} = 19.1 ± 1.2, RZ_{IL} = 13.4 ± 0.6, IBZ_{CL} = 12.1 ± 0.4, IC_{CL} = 10.4 ± 0.6). *p value based on one-way ANOVA followed by Tukey's post hoc test for the intragroup statistical analysis (Total Branch Length: IC vs IBZ_{IL} $p < 0.0001$, IC vs RZ_{IL} $p = 0.0012$; IBZ_{IL} vs RZ_{IL} $p < 0.0001$; IBZ_{IL} vs IBZ_{CL} $p < 0.0001$; IBZ_{IL} vs IC_{CL} $p < 0.0001$; RZ_{IL} vs IC_{CL} $p = 0.0003$; Branches: IC vs IBZ_{IL} $p < 0.0001$, IC vs RZ_{IL} $p = 0.0206$; IBZ_{IL} vs RZ_{IL} $p < 0.0001$; IBZ_{IL} vs IBZ_{CL} $p < 0.0001$; IBZ_{IL} vs IC_{CL} $p < 0.0001$; RZ_{IL} vs IC_{CL} $p = 0.0108$; Junctions: IC vs IBZ_{IL} $p < 0.0001$, IC vs RZ_{IL} $p = 0.0106$; IC vs IBZ_{CL} $p = 0.0143$; IBZ_{IL} vs RZ_{IL} $p < 0.0001$; IBZ_{IL} vs IBZ_{CL} $p < 0.0001$; IBZ_{IL} vs IC_{CL} $p < 0.0001$; RZ_{IL} vs IC_{CL} $p = 0.0320$; IBZ_{CL} vs IC_{CL} $p = 0.0424$). **e** The graphs show total branch length, number of branches, number of actual junctions (merging neighbor junction voxels) with an arbitrary number of projecting branches. All morphological parameters are normalized by the Sham group for both experimental groups (in green PT $n = 6$ and in blue PTRC $n = 6$). The graphs are shown as mean ± SEM. *p value based on two-way ANOVA followed by Tukey's post hoc test for the intergroup statistical analysis (Total Branch Length: PT vs PTRC IBZ_{IL} $p = 0.0010$, PT vs PTRC RZ_{IL} $p = 0.0127$; Branches: PT vs PTRC IBZ_{IL} $p < 0.0001$, PT vs PTRC RZ_{IL} $p < 0.0001$, PT vs PTRC IBZ_{CL} $p < 0.0001$, PT vs PTRC IC_{CL} $p < 0.0001$; Junctions: PT vs PTRC IBZ_{IL} $p = 0.0002$, PT vs PTRC RZ_{IL} $p < 0.0001$, PT vs PTRC IBZ_{CL} $p < 0.0001$, PT vs PTRC IC_{CL} $p < 0.0001$). IC ischemic core, *IBZ_{IL}* ischemic border zone ipsi-lateral, *RZ_{IL}* remote zone ipsi-lateral, *IBZ_{CL}* ischemic border zone contra-lateral, *IC_{CL}* ischemic core contra-lateral.

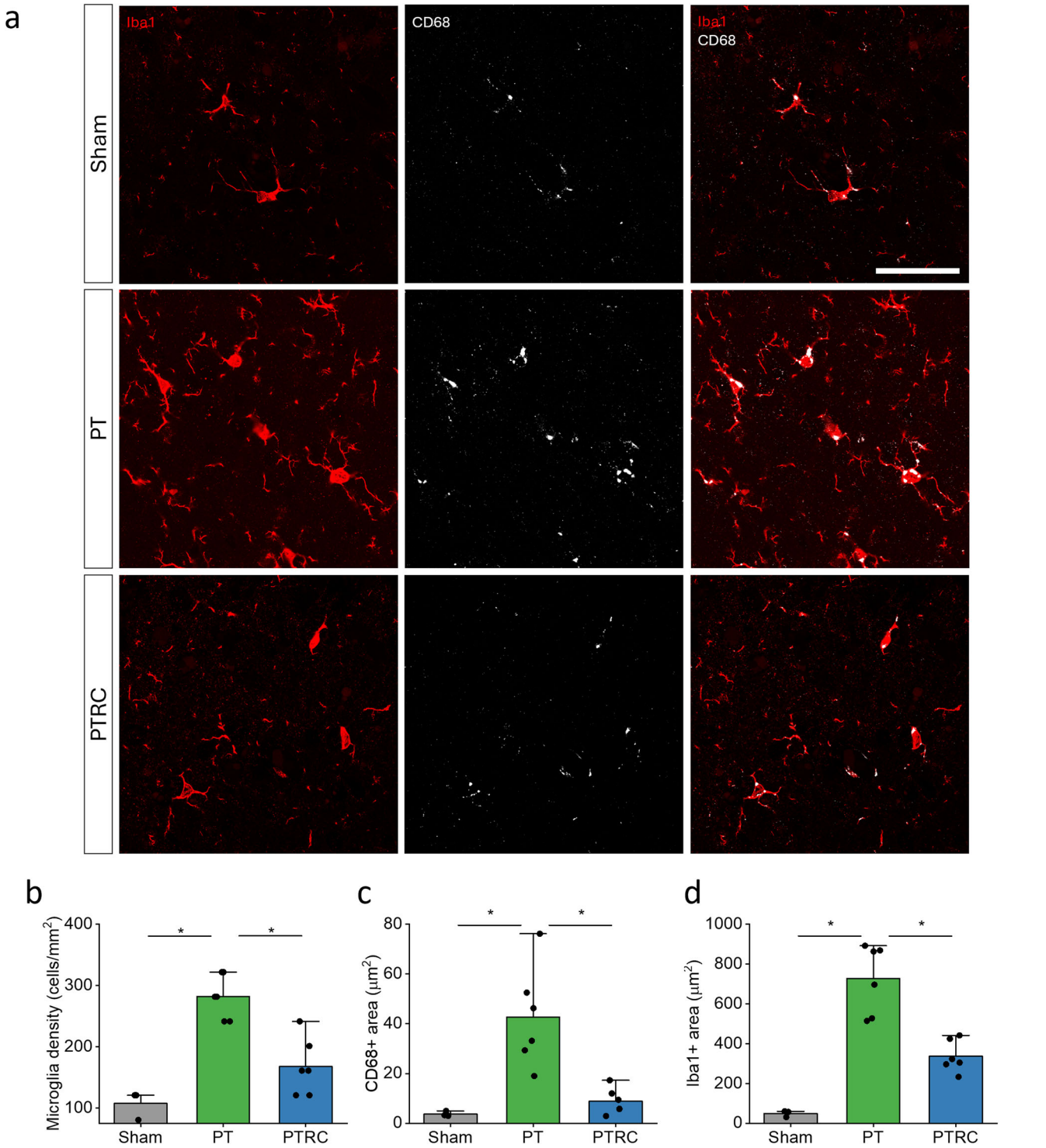

Fig. 5 | Microglia response in perilesioned area. a Representative confocal images for the microglia (Iba1 in red) and phagocytosis activity (CD68 in white). Scale bar 50 µm. **b** The graph shows the microglia density (mean ± SEM) of Iba1-positive cells in the three experimental groups (Sham $n = 3$; PT $n = 6$; PTRC $n = 6$; Sham=107.3 ± 13.41; PT = 281.5 ± 14.69; PTRC = 167.6 ± 19.20). *p value based on one-way ANOVA followed by Tukey's post hoc test for the intragroup statistical analysis ($F_{(2, 12)} = 23.22$ $p < 0.0001$; Sham vs PT $p = 0.0001$; PT vs PTRC $p = 0.0008$). **c** The graph shows the CD68 area (mean ± SEM) in the three experimental groups (Sham $n = 3$; PT $n = 6$; PTRC $n = 6$; Sham = 3.73 ± 0.62; PT = 42.72 ± 8.29; PTRC = 8.84 ± 2.13). *p value based on one-way ANOVA followed by Tukey's post hoc test for the intragroup statistical analysis ($F_{(2, 12)} = 12.57$ $p = 0.0011$; Sham vs PT $p = 0.0041$; PT vs PTRC $p = 0.0026$). **d** The graph shows the Iba1 area (mean ± SEM) in the three experimental groups (Sham $n = 3$; PT $n = 6$; PTRC $n = 6$; Sham = 49.38 ± 9.36; PT = 726.8 ± 71.12; PTRC = 337.0 ± 32.78). *p value based on one-way ANOVA followed by Tukey's post hoc test for the intragroup statistical analysis ($F_{(2, 12)} = 33.00$ $p < 0.0001$; Sham vs PT $p < 0.0001$; Sham vs PTRC $p = 0.017$; PT vs PTRC $p = 0.0004$).

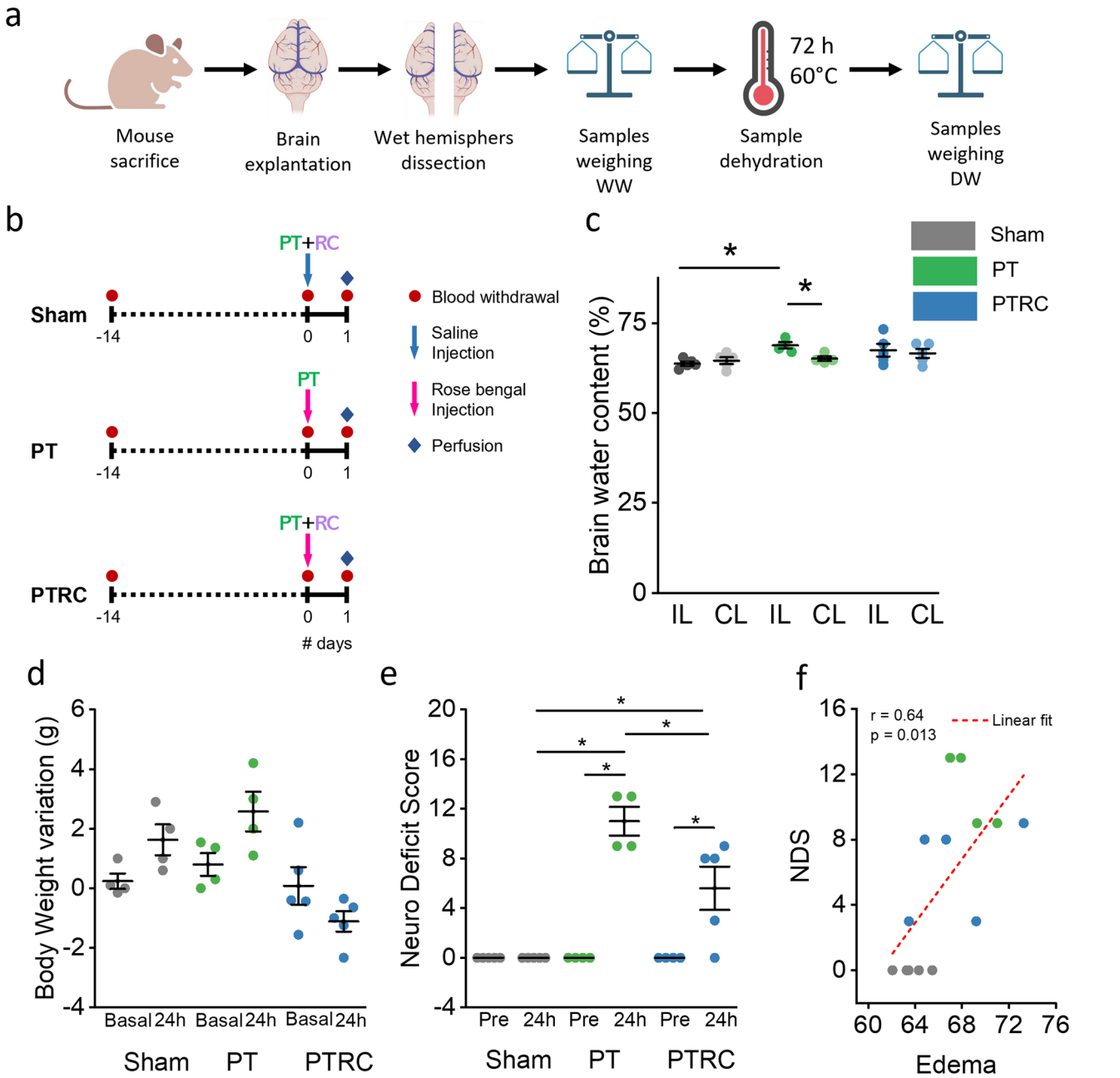

Fig. 6 | Timely recanalization of occluded MCA reduces the insurgence of cerebral edema. a Schematic representation of the experimental procedure to evaluate brain water content. **b** Experimental timeline for the second set of experiments in Sham ($n = 5$), PT ($n = 4$), and PTRC ($n = 5$) mice. **c** The graph shows a comparison between Sham, PT and PTRC groups of brain water content in the left (injured/operated) and right hemispheres. Following mean and SEM values in the different experimental groups: Sham IL = 63.3 ± 0.4 Sham CL = 64.0 ± 0.9; PT IL = 68.8 ± 0.9, PT CL = 65.1 ± 0.6; PTRC IL = 65.9 ± 1.0, PTRC CL = 67.2 ± 1.8. *p value based on Two-way ANOVA ($F_{(5, 22)} = 4.206$) followed by post hoc Tukey HSD test: PT IL-CL p = 0.147; Sham IL-PT IL $p = 0.035$. **d** The graph shows variation in mice weight between pre-stroke conditions and basal time point, and between basal conditions and 24 h after surgery. Following mean and SEM values in the different experimental groups: Sham: basal = 0.4 ± 0.2; 24 h = 1.4 ± 0.5; PT: basal = 0.8 ± 0.4; 24 h = 2.6 ± 0.7; PTRC: basal = 0.1 ± 0.6; 24 h = −1.1 ± 0.3. **e** The graph highlights an increase in neurological deficit scores in the Sham, PT, and PTRC groups 24 h after surgery. Following mean and SEM values in the different experimental groups: Pre: Sham = 0, PT = 0, PTRC = 0; 24 h: Sham = 0; PT = 11 ± 1.1; PTRC = 5.6 ± 1.7. *p value based on Two way ANOVA repeated measure followed by post hoc Tukey HSD test ($F_{(5, 22)} = 50.991$): PT Pre-24h $p < 0.00001$; PTRC Pre-24h $p = 0.004$; Sham 24h-PT 24 h $p < 0.00001$; Sham 24h-PTRC 24 h $p = 0.006$; PT 24h-PTRC 24 h $p = 0.008$. **f** Correlation fit of neuro deficit score and brain water content Pearson correlation r = 0.640; p value = 0.013.

link between pro- and anti-inflammatory proteins modulation and cerebral edema insurgence in the acute phase after the lesion. The analysis of circulating biomarkers in the PT group showed an increase in proinflammatory chemokines and cytokines in the acute phase after the lesion, distinctive of the early phase of the inflammatory response[42]. As previously observed through immunostaining analysis of astrocytes[11], this result confirms that our model of laser-induced occlusion of the distal MCA recapitulates the main inflammation mechanisms induced by ischemia. Moreover, we found that a precocious increment of the antiinflammatory cytokine IL-10 characterizes PT mice. Although the increase in IL-10 has been associated with a neuroprotective effect after cerebral ischemia[43,44], we speculate that the strong inflammation triggered by MCA occlusion in PT mice may overshadow the antiinflammatory effect of IL-10. Finally, we observed that PTRC mice were characterized by a milder inflammatory

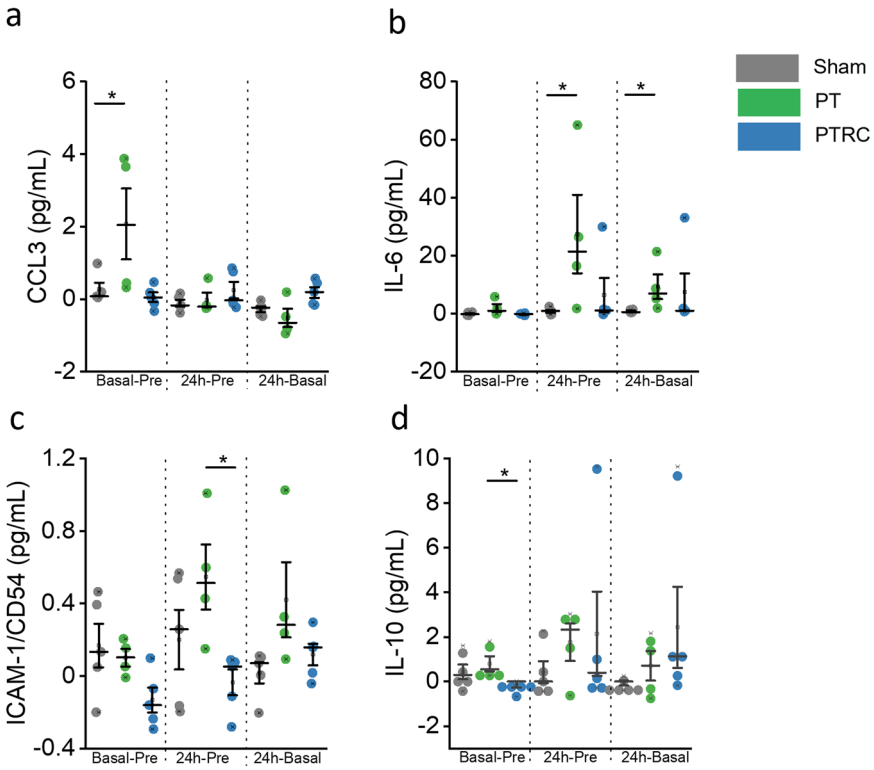

Fig. 7 | Circulating biomarkers analysis reveals a strong proinflammatory response in stroke mice lacking recanalization. a The graph shows the variation of chemokine CCL3 between Basal and Pre, 24 h and Pre, 24 h and Basal time points. *p* value based on Kruskal–Wallis Anova followed by Dunn's Test Basal-Pre Sham-PT $p = 0.0497$. **b** The graph shows the variation of cytokine IL-6 between Basal and Pre, 24 h and Pre, 24 h and Basal time points. *p* value based on Kruskal–Wallis Anova followed by Dunn's Test 24h-Pre Sham-PT $p = 0.0459$; 24h-Basal Sham PT $p = 0.0167$. **c** The graph shows the variation of cytokine ICAM-1/CD54 between Basal and Pre, 24 h and Pre, 24 h and Basal time points. *p* value based on Kruskal–Wallis Anova followed by Dunn's Test 24h-Pre PT-PTRC $p = 0.041$. **d** The graph shows the variation of cytokine IL-10 between Basal and Pre, 24 h and Pre, 24 h and Basal time points. *p* value based on Kruskal–Wallis Anova followed by Dunn's Test Basal-Pre PT-PTRC $p = 0.03$.

reaction that emerges in a delayed time window (24 h after ischemia) compared to PT mice. Indeed, the evaluation of CCL3 and IL-6 expression in PTRC mice showed a similar trend to Sham mice in the Basal-Pre time points comparison. The inflammatory response strongly reduced by recanalization might prevent cerebral edema occurrence.

In conclusion, our findings underscore the importance of controlled reperfusion strategies in stroke management and highlight the potential therapeutic benefits of targeted recanalization. Developing an animal stroke model that closely mimics human ischemic stroke pathophysiology is crucial for finding critical insights regarding the complexities of post-stroke recovery[45,46]. Further elucidation of the underlying mechanisms, including the investigation of neuronal activation features[47,48], structural plasticity on Thy1-GFPM mice, and vascular permeability, may offer novel therapeutic targets for improving stroke outcomes. Furthermore, in the next studies we will create a permanent cranial window that allows optical access to the MCA in order to carry out occlusion and recanalization on an awake mice, reducing the time of anesthesia and brain exposure. Finally, while in this work we dissected some critical aspects of the acute phase after stroke, in particular in the hospital stay time window (5–7 days), future work should focus on optimizing recanalization protocols and targeting the potential synergistic effects of adjunctive therapies such as pharmacological intervention with neuroprotective agents like glyburide[49] to enhance post-stroke recovery.

Collaboration between preclinical and clinical researchers, exemplified by initiatives like the TREES Study group, is indeed crucial for advancing medical research, particularly in areas like stroke treatment. Integrating insights from animal models into clinical practice requires a cohesive approach that bridges the gap between bench and bedside. By fostering this collaboration, researchers can develop more relevant experimental studies that address real clinical needs, ultimately leading to improved patient outcomes.

Methods

Mice

All procedures involving mice were performed in accordance with regulations of the Italian Ministry of Health authorization n. 723/2019. We have complied with all relevant ethical regulations for animal use. Mice were housed in clear plastic cages under a 12 h light/dark cycle and were given *ad libitum* access to water and food. We used a transgenic mouse line, C57BL/6J-Tg(Thy1-EGFP)MJrs/J, from Jackson Laboratories (Bar Harbor, Maine USA). Mice were identified by earmarks and numbered accordingly. Animals were randomly divided into 2 groups (see Supplementary Fig 1a): Lesion experiments: Sham = 3; PT = 6; PTRC = 6; Edema experiments: Sham = 5; PT = 4; PTRC = 5. The PT animals from the first experimental set are the same previously used for the publication by Conti et al. 2023. The data from these animals have been reanalyzed to allow comparison with the newly acquired data from the Sham and PTRC groups. Sham-operated mice were subjected to the same surgery and procedure with respect to PTRC mice except for the Rose Bengal injection, replaced by the injection of the same volume of saline. Each group contained comparable numbers of male and female mice. The age of mice (ranging from 5 to 6-month old) was consistent between groups.

Photothrombotic occlusion and LED recanalization of the distal branch of the middle cerebral artery

The procedure to induce the photothrombotic occlusion of the distal MCA was previously described in our recent work[11,50]. Briefly, mice were anesthetized with ketamine (100 mg/kg) and xylazine (9 mg/kg). Body temperature was maintained at 37 °C with a heating pad (ThermoStar Temperature Controller, RWD, USA). Mice were placed on a surgery pad, lying on one side. Mouse hairs between the eye and the ear were removed and the exposed skin was cleaned with betadine and ethanol. Then, local anesthetic lidocaine 2% (20 mg/mL) was applied. The skin over the squamosal bone was cut, and the muscle was detached from the skull and gently pushed down to expose the bone. We used a dental drill (Silfradent, Forlì-Cesena Italia) to create a small craniotomy over the squamosal bone to expose the distal branch of the middle cerebral artery. Once removed from the flap bone, the photosensitive dye Rose Bengal (0.2 ml, 10 mg/ml solution in Phosphate Buffer Saline (PBS), P3813 Sigma Aldrich, USA) was intraperitoneally injected. To induce photothrombosis, we employed a 532 nm laser (Laser Diode CPS532, Thorlabs, Germany) focused with a 70 mm lens on the targeted blood vessel (laser intensity 128 mW/mm^2). The mouse was

held by the side on a stage allowing displacements in the x-y-z directions (Translation Stage DTS25/M, Thorlabs, Germany). Five minutes after the injection of the dye, the green laser was focused right downstream to the MCA branch for 25 min, to promote the formation of a stable clot and the consequent occlusion of the distal branch of the MCA. Rose Bengal concentration and laser irradiation parameters (power and illumination duration) were determined based on our previous paper[11] This approach ensures a high occlusion success rate because the effective formation of a clot can be monitored through a surgical microscope, allowing the irradiation duration to be precisely adjusted until the vessel is fully occluded, typically after 25 min.

After 30 min of stable occlusion, we illuminated for 15 min the occlusion site with a UV LED (SOLIS-365C, Thorlabs, Germany). High energy 365 nm light is capable of disrupting the fibrine bounds inside the clot and thus producing the recanalization of the blood vessel. The diameter size of the UV light was controlled with a beam expander (GBE02-A, Thorlabs, Germany) and progressively focused with a three-lens system consisting of a 120 mm, 90 mm, and 70 mm lens.

At the end of the procedure, the muscle was placed back over the bone, and the skin was sutured. After surgery mice were placed in their cages and kept warm using a heating pad; mouse general conditions were closely monitored in the following days.

Neurodeficit score evaluation

Motor impairment was assessed using the neurodeficit score, modifying the protocol applied by Balbi and collaborators[51], based on a standardized qualitative assessment for measuring the degree of motor impairment[52]. Briefly, the mouse was placed on a flat surface and gently lifted by the base of the tail until the forepaws were no longer touching the surface. Forelimb and hindlimb flexion were evaluated assigning a score (range 0–2) to mice based on their adduction and flexion capability. Subsequently, the mouse was lifted by its tail and held 15 cm above the flat surface for 10 s to evaluate the C-shaped bending of the body towards one side, bringing its snout close to its hindlimb (score range 0–2). To evaluate grip strength, balance, and endurance we tested mice in the wire hanging test. Mice were brought by the tail near a 2-mm-thick metallic wire maintained 35 cm above a layer of bedding material to prevent injury to the animal in case of falls. When the animal hung to the wire with the forelimb, the mouse was released by the operator. If the animal reached one end of the wire the score was increased by 1. If the animal fell the score was diminished by 1, and the elapsed time was noted. Mice performed three trials to obtain the final score. Forepaw grasping was evaluated by lifting the mouse by its tail and having it grasp a horizontal metal wire of a diameter of 2 mm with the forelimbs (score range 0–3). Before concluding the test procedure, the mouse was placed on a surface and the hindlimbs were gently displaced 1–2 cm laterally. The mouse was scored on the amount of time needed to reposition its hindlimb (score range 0–3). After the neurological evaluation mice were placed in their cage until the subsequent evaluation.

Novel object recognition test

The novel object recognition (NOR) test evaluates the rodents' ability to recognize a novel object in the environment, providing an index of recognition memory. The test is performed on two consecutive days (6 and 7 days post-stroke) and is composed of three phases: habituation, familiarization, and test. Before each session, mice in their cages were brought to the testing room for 30 min to allow the acclimatization to the novel environment. On day 1, habituation, each mouse was allowed to explore an empty arena (45 cm wide × 45 cm long × 30 cm high, methacrylate) for 5 min. On the following day, familiarization, each mouse was placed for 10 min in the arena with two identical cylindrical objects (diameter 4.5 cm × 6.0 cm high) placed at an equal distance of ~10 cm from the wall. We choose two objects of such dimensions to allow mice to climb over the objects providing for a sufficient level of exploration. Double-sided adhesive tape was used to hold the objects to the floor. After this familiarization phase, the mouse was placed back in the acclimatization cage for 5 min. To remove the smell from the object's surface, after each session, the arena and the objects were carefully cleaned with 70% ethanol, dried, and ventilated. Then, during the test, each mouse was placed in the arena in the presence of one of the familiar objects and a novel one (4.5 cm wide × 4.0 cm long × 5.5 cm high) for 15 min. Each session is recorded by a CMOS camera (Chameleon3 USB3, FLIR). The time spent exploring the new object provides an index of recognition memory.

Analysis of novel object recognition test

Raw RGB behavioral recordings acquired at 30 fps were processed using ImageJ[53]. Images were first converted to 8-bit depth and binned (4 × 4, method: average; novel pixel size: 2.3 mm) to decrease file dimensions. For NOR testing phase, a time average projection image of the recording was subtracted from each of the frames, so as to remove the presence of the two objects which could impair mouse detection. Binned images were then thresholded and binarized in order to set to 0 everything except the mouse inside the behavioral arena. A median filter (radius: 3 pixels) was applied to binarized images in order to smooth the edges of the mouse silhouette into a blob-like shape. Couples of *x-y* coordinates of the center of mass of the binarized mouse were then extracted for all the frames of the recording. Mouse interframe displacement was computed applying the Pythagorean theorem to consecutive pairs of center of mass coordinates[54]. The displacement value expressed as the number of pixels was then converted in mm multiplying it for the pixel size.

Mice locomotion characterization was performed using habituation phase recordings. To calculate velocity during locomotion, we first divided mouse inter-frame displacement (surpassing a threshold of 0.58 mm to eliminate localization jitter) by the camera exposure time. The obtained instant velocity values were then averaged. The time the animal spent in movement (locomotion time %) was calculated by counting all the frames surpassing the localization jitter threshold and multiplying the number obtained by the camera exposure time.

For the novel object recognition test two investigation zones (15×15 cm^2) centered on each of the objects (object side/diameter: 5 cm) were defined. Novel object exploration was calculated as the percentage of frames throughout the whole recording in which the center of mass of the animal was inside the novel object investigation zone. Discrimination index (DI) is defined as the time spent investigating the novel object minus the time spent exploring the old object, divided by the sum of the two.

Immunohistochemical analysis

For ex vivo investigation, Sham, stroke-operated, and recanalized mice were transcardially perfused with 4% PFA on day 7 after surgery. Brains were cut using a vibrating-blade vibratome (Leica) to obtain 100-µm-thick coronal sections and contralateral hemisphere respect to the lesion was marked in order to allow the distinction between the two hemispheres. Data concerning PT mice were acquired in a previous set of experiments[11].

The NeuN immunostaining (1:1000; anti-NeuN chicken, ABN91 Millipore) was performed to quantify the lesion volume 1 week after stroke. We analyzed one slice every 300 µm, and the total lesion volume was calculated by summing up all damaged areas and multiplying the number by section thicknesses of 100 µm and by the spacing factor 4. Images were acquired with a 5× objective using a widefield microscope equipped with a structured illumination module (Apotome 3, Carl Zeiss). The total volume in cubic millimeters is given as the mean ± SEM of all analyzed animals (Sham $n = 3$; PT $n = 6$; PTRC $n = 6$). Additionally, we evaluated the impact of the ischemic insult across various anatomical areas of the mouse cortex. This was achieved by superimposing anatomical tables from the Allen Brain Atlas onto the coronal sections. High magnification images of NeuN-stained brain sections were acquired using a confocal fluorescence microscope (Carl Zeiss LSM 900) with a 63× oil-immersion objective.

The immunostaining for glial fibrillary acidic protein (GFAP; 1:1000; anti-GFAP rabbit, ab7260 Abcam) is used to analyze the density and the morphology of the astrocytic population. The number of GFAP-positive

neurons was analyzed using confocal fluorescence microscopes (Carl Zeiss LSM 900 and Nikon Eclipse TE 300) with a 40× oil-immersion objective. We focus our investigation on the following five regions of interest (ROIs): the ischemic core (IC); the peri-infarct area [ischemic border zone ipsilesional (IBZ_{IL})]; a region in the ipsilesional hemisphere distant to the stroke core [remote zone IL (RZ_{IL})]; a region contralateral (CL) to the peri-infarct area [ischemic border zone CL (IBZ_{CL})]; and a region in the healthy hemisphere CL to the ischemic core (IC_{CL}). For each ROI we acquired three fields of view. The density of GFAP-positive cells was evaluated considering the following criteria: (1) the same brightness/contrast value was set for all images; (2) cells placed at the border of the image were not counted; (3) cells that were not clearly visible were excluded and therefore not counted; and (4) nonspecific signals of the background were excluded.

For all the animals, three slices of the brain, central to the damage, were analyzed. In each slice, we acquired three images (159.72 × 159.72 μm) for each of the five ROIs and in each image, we identified one astrocyte.

By applying Sholl's method (ImageJ software), we isolated individual astrocytes, and, starting from the soma, we drew concentric circles around them, at a distance of 3 μm from each other. This method allows quantifying the number of intersections of each astrocytic process with a single circumference and the total number of intersections.

We used Skeleton analysis (ImageJ software) to determine the total length of the processes, the number of branches, the number of junctions, the number of end-points of the branches, the junction voxels, the average branch length, and the maximum branch length of the astrocytes for each ROI.

Microglial cells and phagosomes were stained respectively with ionized calcium-binding adapter molecule 1 (Iba1; 1:500; rabbit anti-Iba1, Wako, Osaka, Japan, 019–19741) and Cluster of Differentiation 68 (CD68; 1:250; rat anti-CD68, BioRad, #MCA1957). Images were acquired with a confocal microscope (Carl Zeiss LSM 900) using a 40× objective with a single z-stack. The central plane of the sample in the z-axis was selected for image acquisition. Three fields of view in the peri-lesioned cortex for each animal were acquired for each experimental group.

For microglial density analysis, images were processed through Fiji Image software: microglia somata in the field of view was counted by the Cell Counter. Density was calculated as the number of soma divided by the area, and expressed as *n* of cells/mm2.

For the quantification of engulfed materials, sequential illumination with 568 nm and 648 nm laser lines was used to detect Iba1 and CD68, respectively. Analysis of engulfed and non-engulfed material was performed via the Fiji Image software to quantify the CD68- and Iba1-positive area in μm^2.

Brain water content evaluation

The evaluation of brain water content was performed following the method previously applied by Kenne and collaborators[14]. 24 h after the occlusion of the MCA, mice were sacrificed with an overdose of anesthetic. The brain was divided along the midline and the contralateral and ipsilateral tissue was weighed right after removal to obtain wet weight (WW). The tissue was then dried at 60 °C for 72 h and weighed to obtain dry weight (DW). Water content was calculated as follows: Water Content = (WW–DW)/(WW × 100).

Circulating biomarkers investigation

To test at different time points (pre-stroke, baseline, and 24 h after the occlusion), we drew blood through the retro-orbital sinus. Mice were anesthetized as previously described, and then manually restrained by grasping the nape. A sterile Pasteur pipette was then placed at the canthus of the eye. With a gentle rotation motion, the pipette was inserted into the membrane and continued rotating until blood flowed inside the pipette. At the end of the procedure, a lidocaine ophthalmic gel was applied to the mouse eye. 0.25 mL of blood was stored in a 1.5 mL tube. After 30 min, the tube was centrifuged at room temperature at 3000 × *g* for 30 min, and the supernatant (blood serum) was stored in aliquots at −80 °C. Circulating levels of cytokines/chemokines (IL-1Beta, IL-6, IL-10, IL-12, TNF-alpha, CCL-3, ICAM-1 and VEGF) were measured by Multiplex Luminex Assay using a custom kit (R&D Systems, Milan, Italy), performed according to the manufacturer's recommended protocol. Briefly, 50 μl of diluted serum and standards were added to each well of the 96-microplate. Fifty μl of diluted microparticle cocktail was added to the wells and, the microplate was incubated at room temperature for 2 h. At the end of incubation, plate was washed three times and after the removal of the liquid, we added 50 μl of diluted Biotin-Antibody cocktail to each well and incubated for 1 h at room temperature. We performed 3 cycles of washing and then, we added 50 μl of diluted Streptavidin-PE to each well and incubated for 30 min at room temperature on the shaker at 800 rpm. After 3 cycles of washing, we added 100 μl of wash buffer and incubated for 2 min at room temperature on the shaker at 800 rpm. Within 90 min, we read the microplate on Bio-Rad analyzer and data was analyzed and reported by using Bioplex software.

Statistics and reproducibility

All the analyses performed of both in vivo and ex vivo experiments were performed blind. All data were independently evaluated by the researchers who performed the experiments and the analysis. No separate statistical analysis was performed based on the animal's sex.

Results were considered statistically significant if their corresponding *p* value was less or equal to 0.05. OriginPro software (OriginLab Corporation) was used for all other statistical analyses.

In the immunohistochemical analysis for the comparison between lesion volume of the two experimental groups two-tailed unpaired *t* test was used.

For intragroup comparison of GFAP analysis one-way ANOVA repeated-measures followed by a post hoc Tukey's HSD multiple comparison test was applied. Normalized ex vivo data were obtained by dividing the raw data of the two experimental groups by the mean of the Sham control group. Data of PT were taken from our previous work[11]. The intergroup statistical analysis was performed through a two-way ANOVA followed by a *post hoc* Sidak's HSD test.

The statistical analysis of neuro deficit score was performed through two-way ANOVA repeated measures followed by a *post hoc* Tukey's HSD multiple comparison test.

The statistical analysis of the novel object recognition test was assessed using one-way ANOVA followed by a *post hoc* Tukey's HSD multiple comparison test.

For Brain Water Content evaluation we performed through Two-way ANOVA followed by post hoc Tukey multiple comparison HSD test. Correlation coefficient between brain water content and neuro deficit score was calculated with Pearson Correlation analysis.

For circulating biomarkers statistical analysis, the comparison between three experimental groups (Sham, PT and PTRC) at three different time points (Basal-Pre, 24h-Pre, 24h-Basal) was performed applying Kruskall Wallis ANOVA followed by Dunn's multiple comparison Test.

Figures 1a, 2, and 6a incorporate illustrations generated with BioRender.com. This research was funded by the Regione Toscana-Bando Ricerca Salute 2018, Grant number 20RSVP for the project "NIMBLE: Integrating novel NeuroImaging Measurements and circulating Biomarkers for the prediction of secondary injury foLlowing strokE: from bench to bedside", by the Fondazione Cassa di Risparmio di Firenze, Grant number SIME 2018/1179 id#24055 for the project "STROKELABED Ictus ischemico acuto: dal laboratorio al letto del malato. Studio di biomarcatori ematici e di neuroimaging come predittori di edema cerebrale, estensione della lesione ischemica e dell'outcome funzionale", by European Union's NextGenerationEU Programme with the I-PHOQS Infrastructure [IR0000016, ID D2B8D520, CUP B53C22001750006] "Integrated infrastructure initiative in Photonic and Quantum Sciences", and the Italian

Ministry for University and Research in the framework of the Advanced Light Microscopy Italian Node of Euro-Bioimaging.

Reporting summary

Further information on research design is available in the Nature Portfolio Reporting Summary linked to this article.

Data availability

All data source underlying plots are provided as Supplementary Data. The data that support the study's findings are available from the corresponding author upon reasonable request.

Received: 5 August 2024; Accepted: 16 June 2025;
Published online: 28 July 2025

References

1. Stoll, G. & Pham, M. Beyond recanalization - a call for action in acute stroke. *Nat. Rev. Neurol.* **16**, 591–592 (2020).
2. Nie, X. et al. Futile Recanalization after Endovascular Therapy in Acute Ischemic Stroke. *BioMed Res. Int.***2018**, 5879548 (2018).
3. Piccardi, B., Biagini, S., Iovene, V. & Palumbo, V. Blood biomarkers of parenchymal damage in ischemic stroke patients treated with revascularization therapies. *Biomark. Insights* **14**, 1177271919888225 (2019).
4. Orset, C. et al. Mouse model of in situ thromboembolic stroke and reperfusion. *Stroke* **38**, 2771–2778 (2007).
5. Howells, D. W. et al. Different strokes for different folks: the rich diversity of animal models of focal cerebral ischemia. *J. Cereb. Blood Flow. Metab.* **30**, 1412–1431 (2010).
6. Fluri, F., Schuhmann, M. K. & Kleinschnitz, C. Animal models of ischemic stroke and their application in clinical research. *Drug Des. Devel. Ther.* **9**, 3445–3454 (2015).
7. Xu, W.-W. et al. Ischemia reperfusion injury after gradual versus rapid flow restoration for middle cerebral artery occlusion rats. *Sci. Rep.* **8**, 1638 (2018).
8. Watson, B. D., Prado, R., Veloso, A., Brunschwig, J.-P. & Dietrich, W. D. Cerebral blood flow restoration and reperfusion injury after ultraviolet laser-facilitated middle cerebral artery recanalization in rat thrombotic stroke. *Stroke* **33**, 428–434 (2002).
9. Yao, H. et al. Photothrombotic middle cerebral artery occlusion and reperfusion laser system in spontaneously hypertensive rats. *Stroke* **34**, 2716–2721 (2003).
10. Kleim, J. A., Boychuk, J. A. & Adkins, D. L. Rat models of upper extremity impairment in stroke. *ILAR J.* **48**, 374–384 (2007).
11. Conti, E., Carlini, N., Piccardi, B., Allegra Mascaro, A. L. & Pavone, F. S. Photothrombotic Middle Cerebral Artery Occlusion in mice: a novel model of ischemic stroke. *eNeuro* https://doi.org/10.1523/ENEURO.0244-22.2022 (2023).
12. Candelario-Jalil, E., Dijkhuizen, R. M. & Magnus, T. Neuroinflammation, stroke, blood-brain barrier dysfunction, and imaging modalities. *Stroke* **53**, 1473–1486 (2022).
13. Pillai, D. R. et al. Cerebral ischemia-reperfusion injury in rats-a 3 T MRI study on biphasic blood-brain barrier opening and the dynamics of edema formation. *J. Cereb. Blood Flow. Metab.* **29**, 1846–1855 (2009).
14. Kenne, E., Erlandsson, A., Lindbom, L., Hillered, L. & Clausen, F. Neutrophil depletion reduces edema formation and tissue loss following traumatic brain injury in mice. *J. Neuroinflammation* **9**, 17 (2012).
15. Kawabori, M. & Yenari, M. A. Inflammatory responses in brain ischemia. *Curr. Med. Chem.* **22**, 1258–1277 (2015).
16. Piccardi, B. et al. Reperfusion Injury after ischemic Stroke Study (RISKS): single-centre (Florence, Italy), prospective observational protocol study. *BMJ Open* **8**, e021183 (2018).
17. Tymianski, M. Role of Neuroprotective Approaches in the Recanalization Era. *Stroke* https://doi.org/10.1161/STROKEAHA.123.044229 (2024).
18. El Amki, M. et al. Neutrophils Obstructing Brain Capillaries Are a Major Cause of No-Reflow in Ischemic Stroke. *Cell Rep.* **33**, 108260 (2020).
19. El Amki, M. & Wegener, S. Improving cerebral blood flow after arterial recanalization: a novel therapeutic strategy in stroke. *Int. J. Mol. Sci.* **18**, 2669 (2017).
20. Nogueira, R. G. et al. Trevo versus Merci retrievers for thrombectomy revascularisation of large vessel occlusions in acute ischaemic stroke (TREVO 2): a randomised trial. *Lancet* **380**, 1231–1240 (2012).
21. Al-Mufti, F. et al. Cerebral ischemic reperfusion injury following recanalization of large vessel occlusions. *Neurosurgery* **82**, 781–789 (2018).
22. Cowled, P. & Fitridge, R. Pathophysiology of reperfusion injury. In *Mechanisms of vascular disease: a textbook for vascular specialists* (ed. Fitridge, R.) 415–440 (Springer International Publishing, Cham, 2020).
23. Binder, N. F. et al. Leptomeningeal collaterals regulate reperfusion in ischemic stroke and rescue the brain from futile recanalization. *Neuron* https://doi.org/10.1016/j.neuron.2024.01.031 (2024).
24. Watson, B. D., Dietrich, W. D., Prado, R. & Ginsberg, M. D. Argon laser-induced arterial photothrombosis. Characterization and possible application to therapy of arteriovenous malformations. *J. Neurosurg.* **66**, 748–754 (1987).
25. Shen, X.-Y. et al. Activation and role of astrocytes in ischemic stroke. *Front. Cell. Neurosci.* **15**, 755955 (2021).
26. Liu, Z. & Chopp, M. Astrocytes, therapeutic targets for neuroprotection and neurorestoration in ischemic stroke. *Prog. Neurobiol.* **144**, 103–120 (2016).
27. Zhou, B., Zuo, Y.-X. & Jiang, R.-T. Astrocyte morphology: diversity, plasticity, and role in neurological diseases. *CNS Neurosci. Ther.* **25**, 665–673 (2019).
28. Conti, E., Pavone, F. S. & Allegra Mascaro, A. L. In vivo imaging of the structural plasticity of cortical neurons after stroke. *Methods Mol. Biol.* **2616**, 69–81 (2023).
29. Baldwin, K. T., Murai, K. K. & Khakh, B. S. Astrocyte morphology. *Trends Cell Biol.* https://doi.org/10.1016/j.tcb.2023.09.006 (2023).
30. Ospel, J., Rex, N., Kandregula, S. & Goyal, M. The vessel has been recanalized: now what?. *Neurotherapeutics* **20**, 679–692 (2023).
31. He, Q. et al. Advancing stroke therapy: a deep dive into early phase of ischemic stroke and recanalization. *CNS Neurosci. Ther.* **30**, e14634 (2024).
32. Conti, E. et al. Translational stroke research review: using the mouse to model human futile recanalization and reperfusion injury in ischemic brain tissue. *Cells* **10**, 3308 (2021).
33. Minetti, A. Unlocking the potential of adeno-associated virus in neuroscience: a brief review. *Mol. Biol. Rep.* **51**, 563 (2024).
34. Allegra Mascaro, A. L. et al. Combined rehabilitation promotes the recovery of structural and functional features of healthy neuronal networks after stroke. *Cell Rep.* **28**, 3474–3485.e6 (2019).
35. Kreuz, T. et al. Latency correction in sparse neuronal spike trains. *J. Neurosci. Methods* **381**, 109703 (2022).
36. Vignozzi, L. et al. Combining Gamma neuromodulation and robotic rehabilitation restores parvalbimin-mediated Gamma function and boosts motor recovery in stroke mice. *bioRxiv* **08**, 608060 (2024).
37. Bai, J. & Lyden, P. D. Revisiting cerebral postischemic reperfusion injury: new insights in understanding reperfusion failure, hemorrhage, and edema. *Int. J. Stroke* **10**, 143–152 (2015).
38. Gu, Y. et al. Cerebral edema after ischemic stroke: Pathophysiology and underlying mechanisms. *Front. Neurosci.* **16**, 988283 (2022).
39. Simats, A. et al. A mouse brain-based multi-omics integrative approach reveals potential blood biomarkers for ischemic stroke. *Mol. Cell. Proteom.* **19**, 1921–1936 (2020).
40. Johnson, M. C., Song, H., Cui, J., Mossine, V. V. & Gu, Z. Development of a method and validation for the quantitation of FruArg in mice plasma and brain tissue using UPLC–MS/MS. *ACS Omega* **1**, 663–668 (2016).

41. Irie, M., Fujimura, Y., Yamato, M., Miura, D. & Wariishi, H. Integrated MALDI-MS imaging and LC–MS techniques for visualizing spatiotemporal metabolomic dynamics in a rat stroke model. *Metabolomics* **10**, 473–483 (2014).
42. Simats, A., García-Berrocoso, T. & Montaner, J. Neuroinflammatory biomarkers: from stroke diagnosis and prognosis to therapy. *Biochim. Biophys. Acta Mol. Basis Dis.* **1862**, 411–424 (2016).
43. Doll, D. N., Barr, T. L. & Simpkins, J. W. Cytokines: their role in stroke and potential use as biomarkers and therapeutic targets. *Aging Dis.* **5**, 294 (2014).
44. Spera, P. A., Ellison, J. A., Feuerstein, G. Z. & Barone, F. C. IL-10 reduces rat brain injury following focal stroke. *Neurosci. Lett.* **251**, 189–192 (1998).
45. Scaglione, A., Conti, E., Allegra Mascaro, A. L. & Pavone, F. S. Tracking the effect of therapy with single-trial based classification after stroke. *Front. Syst. Neurosci.* **16**, 840922 (2022).
46. Cecchini, G. et al. Cortical propagation tracks functional recovery after stroke. *PLoS Comput. Biol.* **17**, e1008963 (2021).
47. Conti, E. et al. Combining optogenetic stimulation and motor training improves functional recovery and perilesional cortical activity. *Neurorehabilit. Neural Repair* **36**, 107–118 (2022).
48. Adam, I., Cecchini, G., Fanelli, D., Kreuz, T., Livi, R., Divolo, M., Allegra Mascaro, L. A., Conti, E., Scaglione, A., Silvestri, L. & Pavone, F. S. Inferring network structure and local dynamics from neuronal patterns with quenched disorder. *Chaos Solitons Fractals* **140**, 110235 (2020).
49. King, Z. A., Sheth, K. N., Kimberly, W. T. & Simard, J. M. Profile of intravenous glyburide for the prevention of cerebral edema following large hemispheric infarction: evidence to date. *Drug Des. Devel. Ther.* **12**, 2539–2552 (2018).
50. Sodero, A. et al. Acute ischemic STROKE – from laboratory to the Patient's BED (STROKELABED): a translational approach to reperfusion injury. Study Protocol. *Transl. Neurosci*. **15**, 20220344 (2024).
51. Balbi, M. et al. Longitudinal monitoring of mesoscopic cortical activity in a mouse model of microinfarcts reveals dissociations with behavioral and motor function. *J. Cereb. Blood Flow. Metab.* **39**, 1486–1500 (2019).
52. Bederson, J. B. et al. Rat middle cerebral artery occlusion: evaluation of the model and development of a neurologic examination. *Stroke* **17**, 472–476 (1986).
53. Schneider, C. A., Rasband, W. S. & Eliceiri, K. W. NIH Image to ImageJ: 25 years of image analysis. *Nat. Methods* **9**, 671–675 (2012).
54. Turrini, L. et al. Multimodal characterization of seizures in Zebrafish Larvae. *Biomedicines* **10**, 951 (2022).

Author contributions

A.L.A.M. conceived the study. E.C., A.L.A.M., and N.C. performed the experiments. E.C., A.M., and L.T. analyzed the data. A.M.G., E.S., B.G. performed circulating biomarkers evaluation and analysis. E.C., A.M., and L.T. generated the figures. E.C., A.M., A.L.A.M. wrote the first draft of the manuscript. E.C., A.M., L.T., A.L.A.M., A.M.G., E.S., B.G., C.Sp., C.Sa., M.B., F.S.P. revised the manuscript. A.L.A.M., M.B., F.S.P. provided funding for the study. All authors contributed to the manuscript revision, read, and approved the submitted version.

Competing interests

The authors declare no competing interests.

Additional information

Supplementary information The online version contains supplementary material available at https://doi.org/10.1038/s42003-025-08398-w.

Correspondence and requests for materials should be addressed to Emilia Conti.

Peer review information *Communications Biology* thanks Mohamad El Amki and the other, anonymous, reviewers for their contribution to the peer review of this work. Primary Handling Editors: Christoph Anacker and Mengtan Xing. A peer review file is available.

Reprints and permissions information is available at http://www.nature.com/reprints

Publisher's note Springer Nature remains neutral with regard to jurisdictional claims in published maps and institutional affiliations.

Open Access This article is licensed under a Creative Commons Attribution-NonCommercial-NoDerivatives 4.0 International License, which permits any non-commercial use, sharing, distribution and reproduction in any medium or format, as long as you give appropriate credit to the original author(s) and the source, provide a link to the Creative Commons licence, and indicate if you modified the licensed material. You do not have permission under this licence to share adapted material derived from this article or parts of it. The images or other third party material in this article are included in the article's Creative Commons licence, unless indicated otherwise in a credit line to the material. If material is not included in the article's Creative Commons licence and your intended use is not permitted by statutory regulation or exceeds the permitted use, you will need to obtain permission directly from the copyright holder. To view a copy of this licence, visit http://creativecommons.org/licenses/by-nc-nd/4.0/.

© The Author(s) 2025